

# Chaotic diffusion in the Gliese-876 planetary system

J. G. Martí,<sup>1,2★</sup> P. M. Cincotta<sup>1</sup> and C. Beaugé<sup>2</sup>

<sup>1</sup>*Grupo de Caos en Sistemas Hamiltonianos, Facultad de Ciencias Astronómicas y Geofísicas, Instituto de Astrofísica de La Plata (CONICET-UNLP), Universidad Nacional de La Plata, Paseo del Bosque S/N, B1900FWA La Plata, Argentina*

<sup>2</sup>*Instituto de Astronomía Teórica y Experimental (IATE), Observatorio Astronómico, Universidad Nacional de Córdoba, Laprida 854, X5000BGR – Córdoba, Argentina*

Accepted 2016 April 26. Received 2016 April 26; in original form 2016 March 14

## ABSTRACT

Chaotic diffusion is supposed to be responsible for orbital instabilities in planetary systems after the dissipation of the protoplanetary disc, and a natural consequence of irregular motion. In this paper, we show that resonant multiplanetary systems, despite being highly chaotic, not necessarily exhibit significant diffusion in phase space, and may still survive virtually unchanged over time-scales comparable to their age. Using the GJ-876 system as an example, we analyse the chaotic diffusion of the outermost (and less massive) planet. We construct a set of stability maps in the surrounding regions of the Laplace resonance. We numerically integrate ensembles of close initial conditions, compute Poincaré maps and estimate the chaotic diffusion present in this system. Our results show that, the Laplace resonance contains two different regions: an inner domain characterized by low chaoticity and slow diffusion, and an outer one displaying larger values of dynamical indicators. In the outer resonant domain, the stochastic borders of the Laplace resonance seem to prevent the complete destruction of the system. We characterize the diffusion for small ensembles along the parameters of the outermost planet. Finally, we perform a stability analysis of the inherent chaotic, albeit stable Laplace resonance, by linking the behaviour of the resonant variables of the configurations to the different sub-structures inside the three-body resonance.

**Key words:** Chaos – diffusion – methods: numerical – celestial mechanics – planets and satellites: dynamical evolution and stability – planets and satellites: formation.

## 1 INTRODUCTION

Planetary systems constitute a paradigm of classical  $N$ -body problems. It has long been known that a general  $N$ -body system with  $N \geq 3$  is not integrable. Arnol'd (1963) showed that a typical near-integrable Hamiltonian system (HS) with more than two degrees of freedom is topologically unstable, even for a negligible value of the perturbation. Thus, given a sufficiently long period of time, the actions in the phase space could diffuse from their initial values and lead to orbital instabilities. However, estimates for the instability time-scales are given just for extremely small perturbations (Nekhoroshev 1977; Chirikov 1979; Cincotta et al. 2014), being exponentially large. General estimates of diffusion time-scales for low-to-moderate perturbations are still lacking.

In planetary systems, the diffusion time-scale may be a strong function of the initial conditions, particularly in the vicinity of mean-motion resonances (MMRs). Thus, how long a system can last until completely destroyed is an unsolved problem with great astronomical interest (Laskar 1989). In HSs, orbital instabilities

(and, consequently, strong chaotic diffusion) are generated by the overlap of resonances (Wisdom 1980), and planetary dynamics are no exception. Although many works in recent times have tried to establish a relationship between chaos and instability (Marchal & Saari 1975; Marchal & Bozis 1982; Chambers, Wetherill & Boss 1996; Smith & Lissauer 2009; Deck, Payne & Holman 2013; Giuppone, Morais & Correia 2013; Ramos, Correia-Otto & Beaugé 2015), no general results have been so far obtained, particularly for the case  $N > 2$ .

As the number of detected exoplanets increased, so did their orbital diversity. Short period with nearly circular orbit planets are supposed to have undergone large-scale orbital migration from beyond the snow line, where giant planets are known to be formed. Many of these short-period planets are so close to their parent star that tidal dissipation would have likely circularized their orbits (Martí & Beaugé 2015). Thus, current orbital parameters of such bodies do not provide a good indicator of their dynamical history.

On the other hand, planets in eccentric orbits are generally believed to have formed on nearly circular orbits and later evolved to their presently observed large eccentricities. Among the proposed mechanisms for producing large eccentricities are a passing binary star (Laughlin & Adams 1998), secular perturbations due to a

\* E-mail: jgmarti@fcaglp.unlp.edu.ar

distant stellar or planetary companion (Ford, Kozinsky & Rasio 2000) and strong planet–planet scattering events (Rasio & Ford 1996; Weidenschilling & Marzari 1996; Jurić & Tremaine 2008; Beaugé & Nesvorný 2012).

Multiresonant configurations are supposed to be a natural outcome of disc-driven planetary migration (Masset & Snellgrove 2001; Morbidelli et al. 2007; Hands, Alexander & Dehnen 2014), and their orbital features are not believed to have been affected by planetary instabilities such as planet–planet scattering or Lidov–Kozai resonance. Thus, their configurations should be more representative of the end product of the formation process, and thus indicative of the stability of ‘dynamically quiet’ systems.

Among the population of resonant and near-resonant systems (Rivera et al. 2010; Fabrycky et al. 2012; Wang, Ji & Zhou 2012; Marti, Giuppone & Beauge 2013; Rowe et al. 2014), a large number has been discovered by the *Kepler* mission. However, some of these are still awaiting confirmation, and several key orbital parameters (including their masses) are not known. Thus, in order to perform a detailed dynamical analysis of resonant systems, it seems preferable to turn to those radial velocity detections in which the inclination of the orbital plane has been (at least qualitatively) estimated. One of the best choices is GJ-876, and will be used as our main target in our analysis of diffusion in extrasolar multiresonant planetary systems.

The GJ-876 system contains, up to date, four confirmed planets orbiting an M-type central star ( $M_*$  from 0.32 to 0.334  $M_\odot$  depending on author). The inner planet (GJ-876 d) is very small, located very close to the star, and dynamically detached from the rest of the system. The three other planets are known to be in the vicinity of a Laplace-type resonance, and have been the subject of several investigations (e.g. Rivera et al. 2010; Baluev 2011; Marti et al. 2013; Batygin, Deck & Holman 2015).

A detailed dynamical analysis of this system was presented in Marti et al. (2013), where it was shown that the multiresonant configuration displayed by GJ-876 is chaotic, albeit long-term stable. In that paper, we presented a series of dynamical maps and found stability limits on the mass ratio of the outer planets as well as precise boundaries on the mutual inclination of the system, inferring that the most likely dynamically relaxed configuration is the coplanar case. Most important, once acknowledged that the system is actually multiresonant, we retrieved specific values for the angular parameters of the planets to ensure a better representation for the plane of initial conditions. In this way, we were able to fix initial angular variables in order to define a representative plane obtained via dynamical considerations, where the Laplace resonance can easily be identified.

In this work we aim to give a qualitative picture of the different chaotic processes (regimes) that can be explored by the three-body resonant configuration depicted by the paradigmatic GJ-876 system. Through this, we want to quantify the variation of the actions of the system, associated with fundamental orbital parameters of the planets, by means of a realistic numerical computation of the diffusion coefficients.

## 2 CHAOTIC DIFFUSION

### 2.1 Summary of resonant perturbation theory

In order to sketch the geometry of resonant dynamics in action space, following Chirikov & Vecheslavov (1993) and Cincotta (2002), let  $\mathbf{I}$  denote the  $N$ -dimensional action vector and  $\boldsymbol{\theta}$  its conjugate canonical  $N$ -dimensional angle, and  $H_0(\mathbf{I})$  the unperturbed integrable non-linear Hamiltonian. Then, the frequency vector  $\boldsymbol{\omega}(\mathbf{I}) = \nabla_{\mathbf{I}} H_0$

is always normal to the unperturbed energy surface  $H_0(\mathbf{I}) = h$ . The resonance condition  $\mathbf{k} \cdot \boldsymbol{\omega}(\mathbf{I}^r) = 0$ , where  $\mathbf{k}$  is a non-zero  $N$ -dimensional vector of integers and  $\mathbf{I}^r$  the resonant action, leads to the resonance surface  $\Sigma_{\mathbf{k}}$ . Thus, on any resonant torus, the resonant vector  $\mathbf{k}$ , is tangent to the energy surface.

Any perturbation to  $H_0(\mathbf{I})$ ,  $\varepsilon V(\mathbf{I}, \boldsymbol{\theta})$ , where  $\varepsilon \ll 1$  and  $V$  is an analytic function introduces variations in the unperturbed actions or global integrals. The latter can be Fourier expanded in the angular variables with coefficients that depend on the actions as

$$\varepsilon V = \varepsilon \sum_{\mathbf{k} \neq 0} V_{\mathbf{k}}(\mathbf{I}) \exp(i\mathbf{k} \cdot \boldsymbol{\theta}).$$

In the single resonance formulation, for sufficiently small  $\varepsilon$  and initial conditions such that the system is close to the resonance  $\mathbf{m} \cdot \boldsymbol{\omega}(\mathbf{I}^r) = 0$ , retaining only the largest (real) term corresponding to the resonant phase,  $\mathbf{m} \cdot \boldsymbol{\theta}$ , averaging out all the remaining ones we get for  $|\mathbf{I} - \mathbf{I}^r| \lesssim 2\sqrt{\varepsilon}$  the local Hamiltonian

$$H(\mathbf{I}, \boldsymbol{\theta}) = H_0(\mathbf{I}) + \varepsilon V_{\mathbf{m}}(\mathbf{I}) \cos(\mathbf{m} \cdot \boldsymbol{\theta}), \quad (1)$$

and thus

$$\dot{\mathbf{I}} = -\frac{\partial H}{\partial \boldsymbol{\theta}} = \varepsilon \mathbf{m} V_{\mathbf{m}}(\mathbf{I}) \sin(\mathbf{m} \cdot \boldsymbol{\theta}). \quad (2)$$

The above relation shows that the variation of  $\mathbf{I}$  has the direction of the resonant vector  $\mathbf{m}$ , tangent to the energy surface.

Since the motion is 1D, it is possible to introduce a canonical local change of coordinates (or local change of basis) around  $\mathbf{I}^r$ :  $(\mathbf{I}, \boldsymbol{\theta}) \rightarrow (\mathbf{J}, \boldsymbol{\psi})$  such that  $\psi_1 = \mathbf{m} \cdot \boldsymbol{\theta}$ , and  $\mathbf{I} = \mathbf{I}^r + \mathbf{m} J_1$ , where  $J_1 \lesssim |\mathbf{I} - \mathbf{I}^r| \sim \mathcal{O}(\sqrt{\varepsilon})$ . Since the resonant Hamiltonian is cyclic in  $\psi_2, \dots, \psi_N$ , we can neglect  $J_2, \dots, J_N$  and then keeping terms up to  $J_1^2$ , it takes the well-known pendulum form

$$H_r(J_1, \psi_1) = \frac{J_1^2}{2M} + V_{\mathbf{m}}(\mathbf{I}^r) \cos \psi_1 \quad (3)$$

where

$$M^{-1} = \sum_{i,j} m_i \left( \frac{\partial \omega_i}{\partial I_j} \right)_{\mathbf{I}^r} m_j,$$

is the inverse of the non-linear mass, assumed to be different from zero. All the  $N - 1$  actions  $J_2, \dots, J_N$  are local integrals of the motion whose numerical values should be zero for  $\mathbf{I}^r$  to be an allowed value for the perturbed motion. While  $J_1$  is the action component in the direction of  $\mathbf{m}$ ,  $J_2$  could be taken normal to the energy surface (in the direction of  $\boldsymbol{\omega}(\mathbf{I}^r) \equiv \boldsymbol{\omega}^r$ ) and thus motion in  $J_2$  could be ignored. The remaining  $N - 2$  components,  $J_3, \dots, J_N$  belong to the  $N - 2$  dimensional manifold, the diffusion manifold, defined by the intersection of the energy and resonance surfaces.

Now, let us discuss a crucial difference between HS with  $N \leq 2$  and  $N > 2$  degrees of freedom.

In low-dimensional non-degenerated HS, for instance  $N = 2$ , the unperturbed energy surface  $H_0(I_1, I_2) = h$  is 1D, just a curve. The resonance surface  $m_1 \omega_1(I_1, I_2) + m_2 \omega_2(I_1, I_2) = 0$  is also 1D. Therefore, the intersection of both, energy and resonance surfaces is a single point,  $(I_1^r, I_2^r)$ , a unique torus, the resonant torus. Then, the motion takes place along the resonant vector  $\mathbf{m}$ , tangent to the energy surface. Thus, due to the dimensionality of the energy surface and the invariant tori, any transition from one torus to another is only possible through all the intermediate tori between them. Thus, the motion under a single resonant perturbation is tangent to the energy surface (curve) and *transverse* to the resonance surface (curve). Since the dense set of resonance surfaces do not intersect each other over the energy surface, large chaos and possibly diffusion is only

possible if the perturbation is large enough such that the overlap of nearby resonances takes place. For very small perturbations, chaos is just confined to the thin chaotic layers around the unperturbed separatrix of any resonance and thus the motion is mostly stable.

For  $N$ -dimensional HS with  $N \geq 3$ , the intersection of energy and resonance surfaces has dimension  $N - 2 \geq 1$ . Now, it is clear that the set of all resonance surfaces intersect over the whole energy surface, leading to the so-called Arnol'd web. Focusing again on an isolated resonance, since the motion is confined to the energy surface and has the direction of  $\mathbf{m}$  ( $J_1$ ), there are  $N - 2$  additional directions where motion could proceed when considering the effects of the perturbing terms in the Fourier expansion of  $\varepsilon V$  (besides the resonant one). For instance, when  $N = 3$ , the remaining direction could be taken *along* the direction of the intersection of the energy and resonance surface. This additional direction for the motion corresponds to the third component of the local action  $\mathbf{J}$ ,  $J_3$ . For  $\varepsilon$  small enough and initial conditions such that  $\mathbf{I} \approx \mathbf{I}^*$ , retaining all (or at least the two largest) perturbing terms in the Fourier expansion (besides the resonant one), a slightly perturbed pendulum model is expected, with a thin chaotic layer instead of a smooth separatrix. And moreover, motion in  $J_3$  – along the resonance – could also take place.

It has been conjectured that any orbit lying in this thin chaotic layer might visit the whole Arnol'd web (Arnol'd 1964). Arnol'd showed the existence of motion along the chaotic layer of a given resonance in a rigorous way, for a rather simple near-integrable 3D Hamiltonian. He proved that for a small enough perturbation it is possible to find a trajectory in the vicinity of the separatrix of a given resonance that connects two points separated by a finite distance, i.e. independent of the size of the perturbation but on a very long time-scale. Arnol'd's proof rests on the existence of a chain of tori along the centre of this resonance that provide a path for the orbit. If these tori are very close to each other, this orbit could transit over the chain. Since every torus in the chain is labelled by an action value, a large but finite variation of this action could take place. This mechanism, which permits motion along the resonance chaotic layer, is known as the Arnol'd Mechanism, while the term Arnol'd diffusion generally refers to a possibly global phase-space instability (Giorgilli 1990; Lochak 1999; Cincotta 2002), that is any (chaotic) orbit might visit the full Arnol'd web in a finite time. However, the problem of how to extend Arnol'd mechanism to a generic Hamiltonian remains unsolved. One of the main difficulties is related to the construction of such a chain of tori.

Regardless of this severe limitation to understand Arnol'd diffusion as a global instability, it was largely assumed that Arnol'd diffusion does occur, and it is responsible for the chaotic mixing in relatively large regions of phase space. Nevertheless, in spite of the mathematical difficulties in dealing with this conjecture as a global instability, a local formulation shows that exponentially large times are necessary in order to observe any appreciable variation of the unperturbed integrals. This suggests that Arnol'd diffusion should be irrelevant in actual systems.

On the other hand, those systems exhibiting a divided phase space, where the chaotic component is relevant (and not only confined to the chaotic layers), the time-scale for any diffusion (not Arnol'd diffusion) would be much shorter but still very long (see for instance Chirikov & Vecheslavov 1993; Giordano & Cincotta 2004), like a power law on the perturbation parameter. In the limit of completely random motion, this time-scale – the inverse of the diffusion coefficient – should go as  $\sim \varepsilon^{-2}$ . When resonance overlap takes place, any description such as the Arnol'd Mechanism is no longer

possible since the connected resonance domains become almost completely chaotic, and the required chain of tori does not exist. Therefore, we should use numerical experiments to quantify any diffusion.

## 2.2 Diffusion

In this section, we discuss the so-called chaotic mixing. In terms of the planetary orbits, roughly speaking, chaotic mixing means that trajectories starting in a very small neighbourhood of a given point in phase space, will lose their memory about initial conditions and, for large enough times, all these trajectories appear uncorrelated. This expected 'random' behaviour could be described as a diffusion process in action space. In the limit of a Brownian type motion, the variance of any action grows linearly with time and thus, a local diffusion coefficient could be defined as the constant rate at which the variance changes with time.

However, in any realistic HS the dynamical behaviour is rather far from a completely random motion. Thus, in order to characterize and quantify diffusion we should proceed with numerical experiments. Assume we are dealing with a 3D HS, which can be described in the following action-angle variables:  $(\mathbf{I}, \boldsymbol{\vartheta})$ . Perform a dynamical map with any chaos indicator over a large set of initial conditions, for instance taking a grid on the  $(I_1, I_2)$  plane, and keeping fixed the values of  $\vartheta_i = \vartheta_i^0$ ,  $i = 1, 2, 3$ , and  $I_3 = I_3^0$ . Any chaos indicator will provide information about the local exponential divergence around any given point of the full phase space, in this case represented by the plane where we let the initial values of the actions vary,  $(I_1, I_2)$ .

With this dynamical information at hand, let us consider an ensemble of  $n_p$  initial conditions in a small neighbourhood of size  $\sigma$  around a given point  $(I_1^*, I_2^*)$  on the plane  $(I_1^0, I_2^0)$  with the very same values for the remaining variables,  $\vartheta_i = \vartheta_i^0$ ,  $I_3 = I_3^0$  and where the indicator reveals an unstable, chaotic behaviour. We integrate the equations of motion for all the  $n_p$  points in the ensemble. The space and time distribution of all the points in  $\sigma$  would give us information about the relevance of diffusion for that point. Moreover, we could compute the time evolution of the space variance of the two action components distributions.

As it was already shown in Cincotta et al. (2014), the above-mentioned variance computation should be done after performing a sequence of canonical transformations to a 'good' set of variables. Indeed, in that work it was shown that using the original set of actions, particularly when the perturbation is small, stable oscillations could hide the slow secular growth of the variance with time and thus the local diffusion coefficient would be largely underestimated. However, this normal form computation to get the appropriate set of variables is not easy to be done in general, and since we will not deal with very small perturbations, we adopt an alternative way (Lega, Guzzo & Froeschl 2003; Guzzo, Lega & Froeschl 2006), to reduce somewhat the effect of oscillations in the drift. The above-mentioned procedure to measure the diffusion in the action plane means considering a section of phase space such that all initial conditions starting in  $\sigma$  should satisfy at a given time  $t$ :

$$|\vartheta_1(t) - \vartheta_1^0| + |\vartheta_2(t) - \vartheta_2^0| + |\vartheta_3(t) - \vartheta_3^0| < \delta_1, \quad |I_3(t) - I_3^0| < \delta_2,$$

with  $\delta_1, \delta_2 \ll 1$ . This procedure, though computational expensive, will effectively reduce the presence of fast periodic oscillations in the time evolution of the action variances.

### 3 HAMILTONIAN MODEL FOR A THREE-BODY RESONANCE

Let us consider a system of three planets (masses  $m_1$ ,  $m_2$ , and  $m_3$ ) orbiting a star  $m_0$  under their mutual gravitational forces. The index is chosen such that the initial semimajor axes satisfy the condition  $a_1 < a_2 < a_3$ .

A canonical set of variables introduced by Poincaré allows us to write the Hamiltonian for the four-body problem. Following Laskar & Robutel (1995), let  $\mathbf{r}_i$  be the astrometric positions of the planets, and  $\mathbf{p}_i$  be the barycentric momentum vectors. The pairs  $(\mathbf{r}_i, \mathbf{p}_i)$  form a canonical set of variables with the Hamiltonian given by

$$H = H_0 + H_{\text{dir}} + H_{\text{kin}}. \quad (4)$$

Here,  $H_0$  is the Keplerian part while the perturbations are given by the two remaining terms.  $H_{\text{dir}}$  is the direct part, and  $H_{\text{kin}}$  is the kinetic part of the Hamiltonian, each expressed in terms of the canonical  $(\mathbf{p}_i, \mathbf{r}_i)$  variables as

$$\begin{aligned} H_0 &= - \sum_{i=1}^3 \left( \frac{p_i^2}{2\beta_i} - \frac{m_0 m_i}{r_i} \right) \\ H_{\text{dir}} &= -\mathcal{G} \sum_{i,j=1, i \neq j}^3 \frac{m_i m_j}{\Delta_{ij}} \\ H_{\text{kin}} &= \sum_{i,j=1, i \neq j}^3 \frac{\mathbf{p}_i \cdot \mathbf{p}_j}{m_0}, \end{aligned} \quad (5)$$

where  $\beta_i = m_0 m_i / (m_0 + m_i)$ ,  $\Delta_{ij} = |\mathbf{r}_i - \mathbf{r}_j|$ , and  $\mathcal{G}$  denotes the gravitational constant. The first term of equation (4) defines the Keplerian motion of each planet around the star, while  $H_{\text{dir}}$  and  $H_{\text{kin}}$  represent the mutual interactions among the planets. The barycentric momentum  $\mathbf{p}_i$  in the four-body problem are defined as

$$\mathbf{p}_i = \frac{m_i}{m_T} \left[ \dot{\mathbf{r}}_i \sum_{j \neq i} m_j - \sum_{j \neq i} m_j \dot{\mathbf{r}}_j \right], \quad (6)$$

where  $\dot{\mathbf{r}}_i$  are the derivatives of the astrometric positions and  $m_T = \sum_{i=0}^3 m_i$ . Since we are assuming co-planar orbits, our system contains a total of six degrees of freedom.

Performing a canonical transformation to the modified Delaunay variables, which for the planar case are given by

$$\begin{aligned} L_j &= \beta_j \sqrt{\mu_j a_j} \\ S_j &= L_j (1 - \sqrt{1 - e_j^2}) \end{aligned} \quad (7)$$

with  $\mu_j = \mathcal{G}(m_0 + m_j)$ , the Keplerian part of the Hamiltonian is simply given by the expression:

$$H_0 = - \sum_{i=1}^3 \frac{\mu_i^2 \beta_i^3}{2L_i^2}. \quad (8)$$

In the vicinity of a Laplace-type resonance, we introduce new angular variables in terms of the primary resonant angles for each of the single resonances:

$$\begin{aligned} \sigma_1 &= 2\lambda_2 - \lambda_1 - \varpi_1 \\ \sigma_2 &= 2\lambda_3 - \lambda_2 - \varpi_2 \\ \Delta\varpi_1 &= \varpi_2 - \varpi_1 \\ \Delta\varpi_2 &= \varpi_3 - \varpi_2. \end{aligned} \quad (9)$$

**Table 1.** Masses and orbital elements for the three planets of GJ-876 involved in the Laplace resonance. The values of the angular variables ( $\varpi$  and  $M$ ) were chosen to minimize the variations of the orbital elements over time, and lead to small-amplitude librations of the resonant angles. The  $(a_3, e_3)$  values correspond to those obtained by the four-planet co-planar fit in Rivera et al. (2010).

Parameter	Orbital parameters for the GJ-876 system		
	Planet c	Planet b	Planet e
$P$ (d)	30.0881	61.1166	124.26
$m$ ( $M_{\text{jup}}$ )	0.7142	2.2756	0.0459
$a$ (au)	0.129 590	0.208 317	0.3343
$e$	0.255 91	0.0324	0.055
$\varpi$ ( $^\circ$ )	0.0	0.0	180.0
$M$ ( $^\circ$ )	240.0	120.0	60.0

The resonant angle of the Laplace resonance may be written in terms of the mean longitudes as

$$\phi_{\text{lap}} = \lambda_1 - 3\lambda_2 + 2\lambda_3. \quad (10)$$

After an averaging process with respect to the short-period terms, the resulting resonant Hamiltonian reduces to a system of four degrees-of-freedom.

## 4 DYNAMICAL MAPS

### 4.1 Numerical setup

For all our numerical runs, we used an  $N$ -body code based on a Bulirsch–Stoer integrator with a variable step-size in order to control the relative error ( $E_r$ ) in each time-step. This value was taken equal to  $E_r = 10^{-12}$ .

We constructed a series of dynamical maps using a rectangular grid of initial conditions in the representative plane  $(a_3, e_3)$ . All other variables, as well as the planetary masses, were taken from Table 1, which correspond to values of the angles that lead to minimum excursions in the eccentricities (see Marti et al. 2013 for details).

The top frame of Fig. 1 reproduces the structure of the phase space in the  $(a_3, e_3)$  representative plane in the vicinity of the 2/1 MMR between  $m_3$  and  $m_2$ . Black symbols correspond to the orbital fits of Rivera et al. (2010) and Baluev (2011), each numerically integrated in order to intersect the representative plane. The dynamical map was constructed with a  $82 \times 82$  grid, and each initial condition was integrated for  $5 \times 10^4$  yr. The plot shows the value of  $\Delta e_3$  obtained during this time-span, with a colour code in the range of  $0.0 < \Delta e_3 < 0.6$ . The region associated to the 2/1 commensurability is clearly seen around  $a_3 \simeq 0.335$  au, while other resonances are also detected for larger semimajor axis. This plot is analogous to fig. 7 of Marti et al. (2013).

Initial conditions identified with red correspond to unstable orbits that lead to a disruption of the system within the integration time-span. Stable orbits in the vicinity of the 2/1 MMR define a horseshoe type region with eccentricity reaching up to  $e_3 \simeq 0.1$ . Close to the stability boundary, the values of  $\Delta e_3$  are relatively large (of the order of 0.2). We also identified, deep inside the resonance domain, a small region characterized by very low eccentricity variations.

The two lower graphs show the semi-amplitude of libration of  $\sigma_2$  (middle plot) and of the Laplace angle  $\phi_{\text{lap}}$  (lower plot). Both show very similar behaviour, indicating that practically all initial conditions within the 2/1 MMR also correspond to motion within the Laplace multiplanet resonance.

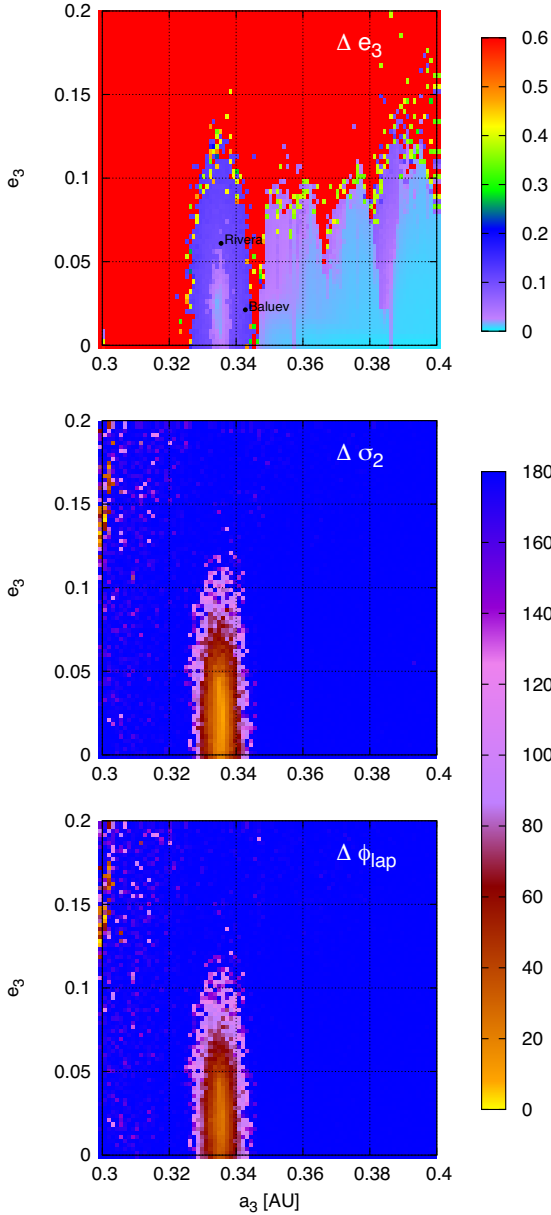


**Figure 1.** Top frame shows a  $\Delta e_3$  dynamical map in the vicinity of the 2/1 MMR between  $m_3$  and  $m_2$  (corresponding to  $a_3 \simeq 0.335$  au). The middle plot shows the amplitude of libration of the primary resonant angle  $\sigma_2$  of the two-body resonant, while the bottom graph shows the amplitude of libration of the Laplace resonance.

Moreover, the region within the Laplace resonance with  $\Delta e_3 \sim 0$  corresponds to small-amplitude librations of its critical argument, as expected.

#### 4.2 Structure of the laplace resonance

In order to realistically assess the chaotic diffusion of this system, we must first define the basic configurations with which to compare the time-evolved parameters.

The best fit for the three-body GJ-876 system is, according to a variety of works (Rivera et al. 2010; Baluev 2011), a chaotic condition; however, it has also been established that the

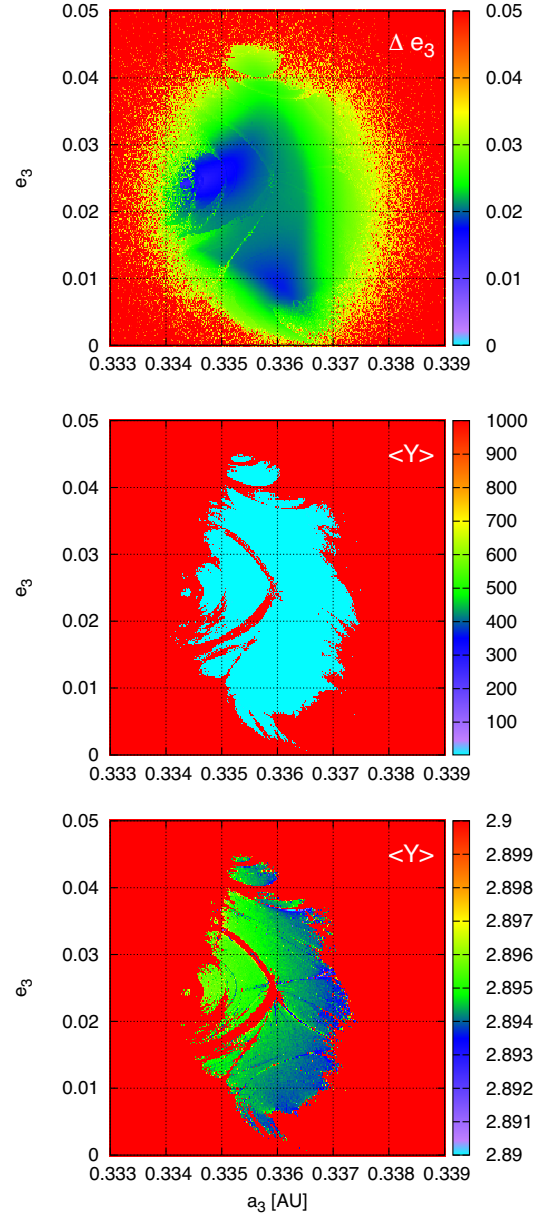


**Figure 2.** Dynamical maps in the representative plane  $(a_3, e_3)$  in the vicinity of the Laplace resonance. The colour code in the top frame corresponds to  $\Delta e_3$  while the two remaining graphs plot values of the MEGNO indicator  $\langle Y \rangle$ .

configuration is stable and locked in a resonant state for extremely long time-scales. In Martí et al. (2013), we presented a thorough exploration of the parameter space, yielding several dynamical constrains.

For instance, we concluded that both dynamical tests and stability considerations point towards a co-planar configuration. We also showed that finite masses are necessary in order to guarantee stability, and estimated upper bounds for the mass ratio. Here, we expand on those results and discuss in more details the evolution of both regular and chaotic orbits with a higher resolution.

Fig. 2 presents new dynamical maps for the central region of the Laplace resonance, corresponding to low-amplitude librations of  $\phi_{\text{lap}}$ . Since we are interested in a detailed analysis of the resonance

structure, we increased the resolution to a  $300 \times 250$  grid of initial conditions in the  $(a_3, e_3)$  plane. The total integration time was also increased to  $10^5$  yr. The values of  $\Delta e_3$  for each initial condition are shown in the top panel, with a colour code in the range of  $0.0 < \Delta e_3 < 0.06$ .

It is important to recall that  $\Delta e_3$  is not a chaotic indicator (e.g. Ramos et al. 2015), although it constitutes an important tool with which to map changes in the structure of the phase space, such as those stemming from separatrix crossings. The Mean Exponential Growth of Nearby Orbits (MEGNO) indicator (Cincotta & Simó 2000; Cincotta, Giordano & Simó 2003), on the other hand, is a robust and efficient chaos indicator.

The middle panel of Fig. 2 shows the same map although this time the colours correspond to the MEGNO values  $\langle Y \rangle$ , where 2 the lowest value, indicates regular motion. We note a very sharp transition between moderate values close to 2 deep within the libration domain, and highly chaotic motion with  $\langle Y \rangle \geq 1000$ . The low-MEGNO region is located in the core of the resonant domain and corresponds to small-amplitude librations of the Laplace angle, as discussed in Fig. 1.

Although both indicators do not show exactly the same results, they share some qualitative features. In both cases, the phase space appears separated into two distinct regions: a moderately regular ( $\langle Y \rangle < 3$ ) domain surrounded by a significantly more chaotic region identified with  $\langle Y \rangle > 10$ . Hereafter, we will refer to each as the *inner* and *outer* resonant domains, respectively.

The lower frame presents, once again, a MEGNO colour map, only this time limited to values found in the inner core of the resonance. We can now see a number of dynamical structures deep within this commensurability. Although similar structures may also be seen in the  $\Delta e_3$  map, these are not so clearly defined. A second interesting result of the MEGNO map is that all initial conditions appear chaotic (reaching a minimum value of  $\langle Y \rangle \simeq 2.89$ ), even for very low amplitudes of libration. Moreover, this figure clearly shows the very signatures of high-order resonances within this domain as narrow channels or simply as smooth curves (see below).

This general chaoticity is not unexpected. Indeed, Nesvorný & Morbidelli (1999) considered the full three-body resonance as a configuration in the SS system (asteroid, Jupiter, and Saturn), in which the time derivative of a generic resonant angle  $\sigma$  satisfies

$$\dot{\sigma} = j_1 \dot{\lambda}_1 + j_2 \dot{\lambda}_2 + j_3 \dot{\lambda}_3 + l_1 \dot{\varpi}_1 + l_2 \dot{\varpi}_2 + l_3 \dot{\varpi}_3 \approx 0, \quad (11)$$

where  $\lambda_i$  and  $\varpi_i$  denote the mean and perihelion longitudes, respectively. The indexes  $(j_1, j_2, j_3) \in \mathbb{Z}^3 \setminus \{0\}$  and  $(l_1, l_2, l_3) \in \mathbb{Z}^3$  are conditioned by D'Alembert's rule:

$$\sum_{i=1}^3 (j_i + l_i) = 0. \quad (12)$$

For a specific three-body MMR (i.e.  $\dot{\lambda}_i = n_i$  yields a fixed value of  $a_i$ ), equation (11) defines several multiplets associated to different vectors of integers  $\mathbf{I}$ , each located at slightly different resonant values of the corresponding semimajor axis. These multiplets (or sub-resonances) will inevitably overlap, generating an extended chaotic region in the three-body resonance. The full  $(j_1, j_2, j_3)$  MMR Hamiltonian  $(P_1, P_2, P_3)$ , up to second order in the eccentricity of the small body ( $P_3$ ), can be reduced to a 4D one. Indeed, after defining

$$\mathbf{I} = (N_3, S_1, S_2, S_3), \quad \boldsymbol{\theta} = (\phi, \varpi_1, \varpi_2, \varpi_3), \quad (13)$$

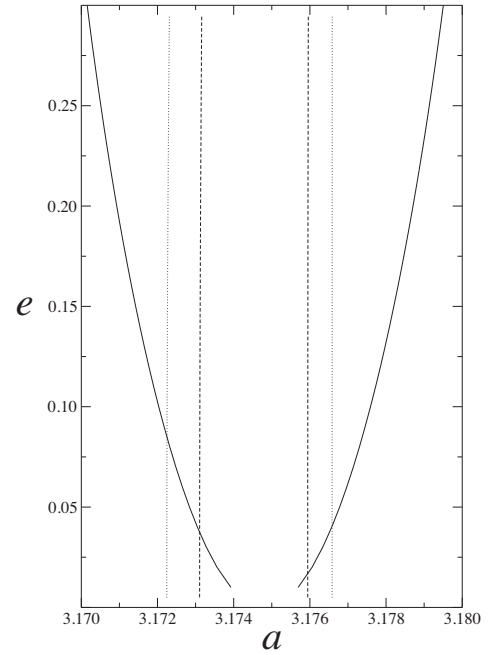


**Figure 3.** Three resonances model for the  $(5, -2, -2)$  three-body MMR. The strength of each resonances is given by the corresponding width. The largest one corresponds to the resonance  $(5\lambda_J - 2\lambda_S - 2\lambda - \varpi)$  while the smallest one to  $(5\lambda_J - 2\lambda_S - 2\lambda + \varpi_S)$ .

where  $\phi = j_1 \lambda_1 + j_2 \lambda_2 + j_3 \lambda_3$  and  $N_3 = L_3/j_3$ , then following the approach of Section 2, the local Hamiltonian reads

$$H(\mathbf{I}, \boldsymbol{\theta}) = -\frac{1}{2j_3^2 N_3^2} - \beta_0 \left(1 + \frac{S_3}{j_3 N_3}\right)^2 + (j_1 n_1 + j_2 n_2) N_3 + \nu_1 S_1 + \nu_2 S_2 + V(\mathbf{I}, \boldsymbol{\theta}), \quad (14)$$

where  $\beta_0 \sim e_3^2$ ,  $\nu_{1,2}$  are perihelion motions of  $P_1$  and  $P_2$  massive planets, respectively. The perturbation takes the form:

$$V(\mathbf{I}, \boldsymbol{\theta}) = \sum_{\mathbf{l}} \beta_{\mathbf{l}}(\mathbf{I}) \cos(\phi + l_1 \varpi_1 + l_2 \varpi_2 + l_3 \varpi_3), \quad (15)$$

and the small coefficients  $\beta_{\mathbf{l}}(\mathbf{I})$  can be given in terms of a power series of the small body's eccentricity (see Nesvorný & Morbidelli 1999).

Considering three different multiplets of the asteroidal three-body resonance  $(5, -2, -2)$ , Cachucho, Cincotta & Ferraz-Mello (2010) applied Chirikov's diffusion theory to investigate, among other effects, variations of the eccentricities of the (490) Veritas family. They clearly show that it is necessary to consider at least the three strongest terms in (15) in order to explain the observed distribution of eccentricities of this asteroidal family. This multiplet of three resonances for this particular MMR in the SS, given by  $\mathbf{I} = (-1, 0, 0), (0, -1, 0), (0, 0, 1)$ , is represented in Fig. 3.

This simple model shows that the three resonances are in overlap and thus the full domain of the MMR is expected to be chaotic and therefore diffusion might occur. Moreover, the above figure allows us to say that diffusion *along* the resonance corresponds to variations of the eccentricity while diffusion *across* the resonance measures variations of the semimajor axis.

In the case of Gliese-876,  $m_3 \ll m_1 < m_2$ , and since we are dealing with the full 4D resonant Hamiltonian in a small domain around Laplace resonance, a dense set of resonances of the form

$$\dot{\phi}_{\text{lap}} + l_1 \dot{\varpi}_1 + l_2 \dot{\varpi}_2 + l_3 \dot{\varpi}_3 \approx 0$$

would appear as well as many other nearby MMR. Thus, regular motion is not expected in this region but a very complex domain of overlap of many resonances. Therefore, the only way to investigate diffusion is by numerical experiments.

In order to understand the structure of the Laplace resonances and the role of the different resonances in the multiplet in the diffusion process, let us write the Hamiltonian in Chirikov's style, taking again the same variables as defined in (13) with  $\phi = \phi_{\text{lap}}$ . Due to the D'Alembert's rule for the Laplace resonance, the harmonic vector  $\mathbf{m} \equiv (1, 0, 0, 0)$  should be resonant, thus we take the angle  $\mathbf{m} \cdot \boldsymbol{\theta} = (\lambda_1 - 3\lambda_2 + \lambda_3)$  as the resonant one. Taking away from the perturbation the resonant term, the Hamiltonian becomes

$$H_r(\mathbf{I}, \boldsymbol{\theta}) = -\frac{1}{2j_2^2 N_3^2} - \beta_0 \left(1 + \frac{S_3}{j_3 N_3}\right)^2 + (j_1 n_1 + j_2 n_2) N_3 + v_1 S_1 + v_2 S_2 + \beta_m(\mathbf{I}) \cos(\mathbf{m} \cdot \boldsymbol{\theta}) + V, \quad (16)$$

where  $V$  includes all terms of the form  $\cos(\phi_{\text{lap}} + l_1 \varpi_1 + l_2 \varpi_2 + l_3 \varpi_3)$  with  $l_i \neq 0$ . Following the formulation of Section 2.1, a canonical transformation or local change of basis  $(\mathbf{I}, \boldsymbol{\theta}) \rightarrow (\mathbf{J}, \boldsymbol{\psi})$  such that

$$\psi_k = \sum_{i=1}^4 \mu_{ik} \theta_k, \quad I_s = I_s^r + \sum_{k=1}^4 J_k \mu_{ks},$$

where  $\mu_{ik}$  are the coefficients of the transformation with  $\mu_{1k} = m_k$ ,  $\mu_{2k} = \omega_2^r / |\boldsymbol{\omega}^r|$ ,  $\dots$ , (so  $\psi_1 = \mathbf{m} \cdot \boldsymbol{\theta}$ ), allows one to reduce the resonant Hamiltonian to

$$H(\mathbf{J}, \boldsymbol{\psi}) = \frac{J_1^2}{2M} + |\boldsymbol{\omega}^r| J_2 + \sum_{s=1}^4 \sum_{k+s>2}^4 \frac{J_k J_s}{2M_{ks}} + \beta_m(I^r) \cos \psi_1 + \sum_l \beta_l(I^r) \cos(\mathbf{l} \cdot \boldsymbol{\theta}(\boldsymbol{\psi})), \quad (17)$$

where  $M$  is the non-linear mass defined in Section 2.1 while the  $M_{ks}$  are similar constants to  $M$  but involving different coefficients of the basis transformation ( $\mu_{ik}$ ) and  $I^r$  is the resonant action that satisfies the resonance condition

$$n_1(I^r) - 3n_2(I^r) + 2n_3(I^r) = 0.$$

Recalling that the dot product is invariant, the replacement  $\boldsymbol{\theta} \rightarrow \boldsymbol{\psi}$  is easily done since  $\mathbf{l} \cdot \boldsymbol{\theta} = \mathbf{r} \cdot \boldsymbol{\psi}$ , where now the components of  $\mathbf{r}$  are real numbers.

Keeping only the actual resonance ( $\phi_{\text{lap}}$ ) and neglecting all the perturbation terms  $\beta_l(I^r)$  for all  $\mathbf{l}$ , the components  $J_2, J_3, J_4$  become local integrals of motion whose value is equal to zero if  $I^r$  is a point of the orbit. Then, the Hamiltonian reduces to a pendulum-like model

$$\tilde{H}_r(J_1, \psi_1) = \frac{J_1^2}{2M} + V(I^r) \cos \psi_1. \quad (18)$$

Thus, the motion *across* the resonance is given by  $J_1$ , the pendulum action. It librates or circulates depending on the value of  $\tilde{H}_r$  and for  $\tilde{H}_r = V(I^r)$  the system lies at the separatrix. When switching on the perturbation ( $\beta_l(I^r) \neq 0$ ), the main effect to the pendulum model is to produce a distortion of the separatrix and the motion in the neighbourhood of this asymptotic trajectory becomes chaotic leading to the so-called chaotic layer. However, a non-vanishing perturbation, including at least two perturbing terms, also leads to variation of the unperturbed local integrals  $J_2, J_3, J_4$ , after a simple inspection of (17). The variation of  $J_2$  has a direction normal to the energy surface and thus it can be ignored. Changes in  $J_3$  and  $J_4$  lie in the diffusion space and therefore *along* the resonance. In other

words, due to the particular geometry of the resonance (see Fig. 3),  $J_1$  measures diffusion in the semimajor axis of  $P_3$  while,  $J_3$  and  $J_4$  lying in the diffusion space, take into account diffusion in the eccentricity of the small body.

From the above discussion it becomes clear that if  $\mathbf{m} \cdot \boldsymbol{\theta} = (\lambda_1 - 3\lambda_2 + \lambda_3)$  is a resonant angle, then  $(\lambda_1 - 3\lambda_2 + \lambda_3 + l_1 \nu_1 + l_2 \nu_2 + l_3 \nu_3)$  is also resonant for any integers  $l_i \neq 0$  that satisfy the D'Alembert's rule. And as we have already shown, all these resonances are overlapping since all of them have almost the same  $I^r$  (or  $a^r$ ). Hence, we expect a fully chaotic domain within the Laplace resonance and therefore diffusion in both directions, along and across the resonance. Moreover, since many other MMR are very close to this Laplace resonance, a large chaotic sea should surround it. As can be seen in Fig. 2, the correspondence between the simple model and the full numerical experimentations is, at least qualitatively, most evident. All this is what we observe in Fig. 2. However, from the above discussion, nothing could be said about the diffusion rate or if the diffusion has a normal character.

## 5 DIFFUSION INSIDE THE LAPLACE RESONANCE

Having analysed the general structure and chaoticity of the Laplace resonance, our next step is to estimate the diffusion times in the different regions within this commensurability.

We performed a series of integrations of ensembles of initial conditions at specific locations in the  $(a_3, e_3)$  plane. Each ensemble consisted of a total of 256 initial conditions, all centred around a given point in the plane, and defining very narrow regions of at most  $10^{-3}$  in  $\Delta e_3$  and  $2 \times 10^{-4}$  in  $\Delta a_3$ . Each initial condition was again integrated for a total time of  $2 \times 10^5$  yr, twice longer than the time-span used for the original map.

During the evolution, we kept a record of every time the particles crossed the representative plane. This was said to occur when the following conditions were satisfied:

- (i)  $\sum_{i=1}^3 (|M_i - M_i^0| + |\varpi_i - \varpi_i^0|) < \epsilon_{\text{ang}}$ ,
- (ii)  $\sum_{i=1}^2 |e_i - e_i^0| < \epsilon_e$ ,
- (iii)  $\sum_{i=1}^2 |a_i - a_i^0| < \epsilon_a$ ,

where  $\epsilon_{\text{ang}}$ ,  $\epsilon_e$ , and  $\epsilon_a$  are predefined values. For this set of simulations, we adopted  $\epsilon_{\text{ang}} = 6^\circ$ ,  $\epsilon_a = 0.005$  au and  $\epsilon_e = 0.005$ .

We integrated a set of nine ensembles (hereafter referred to as 1S, 2S,  $\dots$ , 9S). The first was located in the outer resonant region, while the other ensembles were placed inside the inner resonant region.

Fig. 4 shows the evolution of each ensemble in the representative plane, superimposed with the resonant structure as determined by the  $\Delta e_3$  indicator. The initial conditions are indicated with black rectangles while their subsequent diffusive evolution is depicted in colours.

As seen from the left-hand plot, the S1 ensemble suffers a large-scale diffusion, rapidly covering all the outer resonant region. Motion is highly chaotic and the times between crossings are unpredictable. More interesting, all intersections with the representative plane occur in the red region, which appears detached from the inner resonant zone indicated in green and blue.

The remaining frames in Fig. 4 correspond to initial conditions in the inner resonant zone. In all cases the diffusion is very localized, at least compared with the evolution of 1S. Moreover, the time evolution of the ensembles never leave the inner domain, indicating no noticeable mixing between both parts. This seems to suggest that perhaps both regions are dynamically unconnected (at least

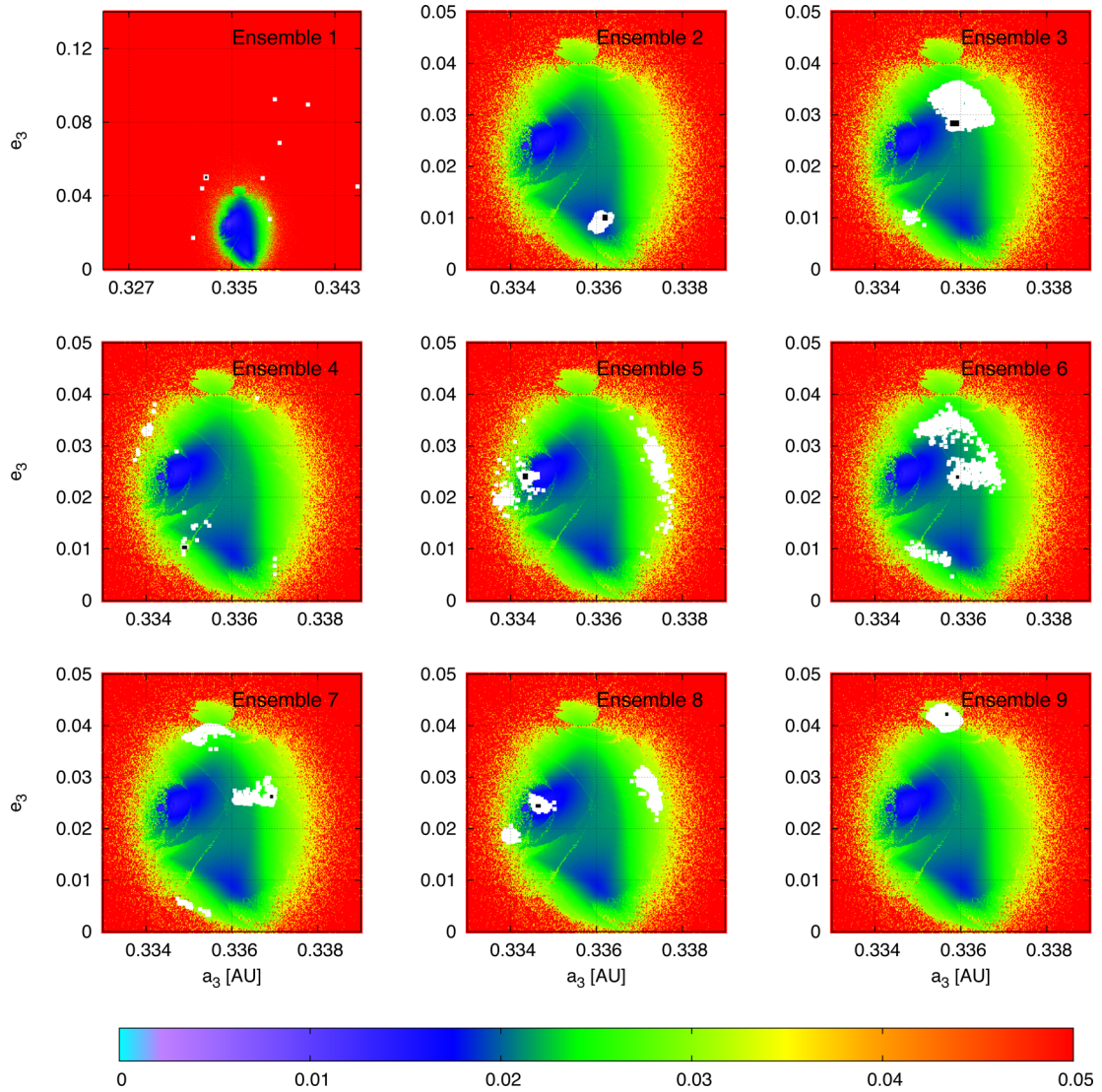


**Figure 4.** Diffusion of 9 ensembles of 256 initial conditions defined in different regions of the representative plane. Total integration time was  $2 \times 10^5$  yr. Black rectangles show the location of the initial ensembles, while the colour dots indicate their diffusion during this time-span.

up to the considered length of the simulations) and that the limit between them could represent a kind of dynamical boundary inside the resonance. In consequence, initial conditions within the inner region seem to be characterized by very small diffusion rates. The opposite seems to occur for initial conditions in the outer domain.

### 5.1 Diffusion coefficients

In this Section, we proceed to quantify the different chaotic regimes within the Laplace resonance. To this end we take advantage of the ensembles 1S to 9S described in the previous section to ensure a sufficiently representative ensemble to compute the variances in both  $a_3$  and  $e_3$ . The ensembles labelled as  $i = 2, \dots, 9$  have a considerable number of intersections with the  $(a_3, e_3)$  plane that ensure a sufficiently good approximation to the actual experimental value of the variance of  $(a_3, e_3)$ . In the case of S1, we already noticed the difficulty of having a significant amount of crossings with the representative plane.

The numerical computation of the variance proceeds as follows.

(i) We sub-divided the total integration time of the ensembles (i.e.

$T_{\text{tot}} = 2 \times 10^5$  yr) into  $N_i$  time intervals of fixed length  $T_{\text{imp}}$ , so that  $T_{\text{imp}} = T_{\text{tot}}/N_i$ . (ii) At each time interval  $[(i-1)T_{\text{imp}}, iT_{\text{imp}}]$ ,  $i = 1, \dots, N_i$  we computed the total plane crossings conditions ( $N_i$ ) which occur at shorter times than the extreme value of the time interval (i.e. if  $T_{\text{cr}} < iT_{\text{imp}}$ ). (iii) A representative value of the variances both for  $a_3$  and  $e_3$  is calculated using all the plane crossing conditions in each time interval following

$$\sigma_x = \frac{1}{N_i} \sum (x(T_{\text{cr}}) - x_0)^2, \quad (19)$$

where  $x$  should be replaced by any of the fundamental parameters  $a_3$  or  $e_3$ , and  $x_0$  is either the semimajor axis  $a_3$  or the eccentricity  $e_3$ , at the centre of the ensemble.

Diffusion processes are commonly characterized by a power-law relationship of the form  $\sigma^2(t) = ct^\alpha$ , with  $c > 0$ . If  $\alpha = 1$  we have normal diffusion, while in case of  $\alpha < 1$  the phenomenon is called sub-diffusion, or when  $\alpha > 1$  it is called superdiffusion. In the normal diffusion case, that corresponds to purely random motion, it is possible to define a numerical diffusion coefficient,  $D$ , as the constant rate at which the variance grows with time. The



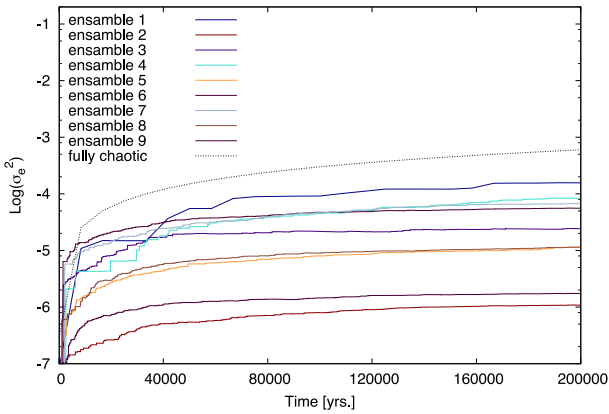


**Figure 5.** Variance of the eccentricity as function of time, obtained for each of the ensembles 1S to 9S. The  $\sigma_e$  values are shown in logarithmic scale in order to see how each curve moves away from the Normal Diffusion curve, depicted in dashed black line on the plot.

computation of the diffusion coefficient in case of sub-diffusion or superdiffusion for a generic HS is yet an open and difficult problem. Therefore, in this work we focus on which type of diffusion dominates the different regions of the resonance discussed above.

Thus, we associate to  $\sigma_x^2$  a power law

$$\sigma_x^2(t) = c_x t^{\alpha_x}, \quad (20)$$

where  $c_x$  and  $\alpha_x$  are the fitted parameters. In case of an exponent  $\alpha \approx 1$  the parameter  $c_x$  is an estimate of the actual and standard diffusion rate coefficient,  $D_x$ . On the other hand, if  $\alpha$  is far from 1, nothing could be said about the diffusion coefficient. Only a qualitative description about the diffusion processes in phase space could be provided.

In Fig. 5, we show the time evolutions of  $\sigma_e$  for each of the ensembles 1S–9S. We also include in the figure the corresponding time evolution for the completely random case ( $\sigma^2 \propto t$ ) just for the sake of comparison. The figure shows that in all cases the nine ensembles have a smaller rate than the expected one for normal diffusion. The ensemble 1S, taken in the outer part of the resonance, presents some similarities with the normal case. For the rest of the ensembles, the 4S shows the highest rate of evolution at large times, but the computed variance for this ensemble is one order of magnitude less than that for the ensemble 1S. This result clearly shows that the inner region of the resonance, while chaotic, presents a dynamical behaviour that looks almost stable and therefore the diffusion, is not well approximated as a Brownian type motion. In Table 2, we show the values of these exponents for the nine ensembles. Clearly only the ensembles 1S and 4S present an exponent close to 1. The

**Table 2.** Exponents  $\alpha$  calculated by a least-squares fit for the data obtained by the variances from each of the nine ensembles.

Ensemble	$\alpha$
1S	0.942 715
2S	0.585 784
3S	0.494 802
4S	0.923 109
5S	0.648 737
6S	0.448 689
7S	0.686 534
8S	0.592 316
9S	0.462 431

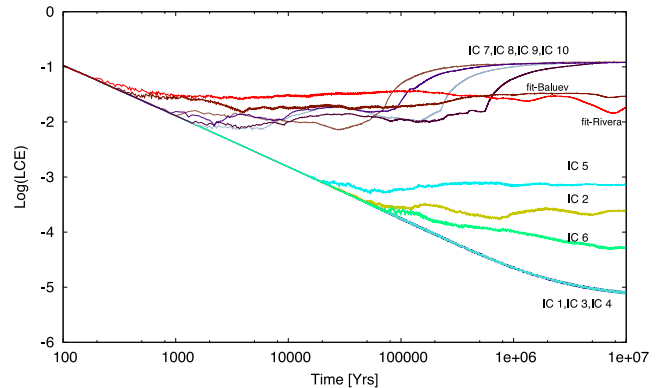
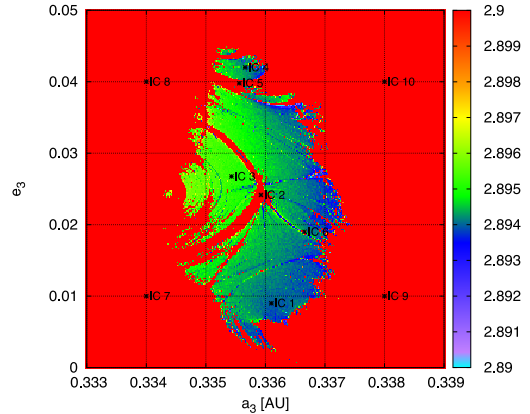


**Figure 6.** Bottom frame shows the Maximum Lyapunov Coefficient (LCE) for 10 initial conditions chosen in different regions of the representative plane (identified in top graph).

associated diffusion coefficient, obtained by a linear fit for  $t \gtrsim 10^4$  yr results  $D \sim 10^{-9}$  for both ensembles. The rest of the ensembles are highly sub-diffusive and thus the dynamical behaviour is rather stable at least for  $t = 2 \times 10^5$  yr. The particular case of ensemble 4S might be explained since its initial position  $(a_0, e_0) \approx (0.335, 0.01)$  is also in the outer region of the resonance but very close to the boundary defined by the MEGNO computation (see for instance Fig. 6). Initially the evolution of the ensemble shows a sub-diffusive behaviour but, for moderate times, the diffusion becomes more normal and maybe for larger times it could reach higher values of the eccentricity.

In this direction, Batygin et al. (2015) developed a 2D model and studied the diffusion on this same system. Besides the difference between the analytic and numerical approximations, they assume a normal diffusion to derive a diffusion coefficient. Our approach shows that this assumption for diffusion in a multiresonant system such as GJ-876 is not well suited, at least in the inner region of the Laplace resonance.

## 6 ORBITAL STABILITY IN THE INNER AND OUTER RESONANT REGIONS

Finally, we wanted to analyse the orbital stability and dynamics of a set of initial conditions in both regions of the Laplace resonance. Fig. 6 shows the Lyapunov characteristic exponent (LCE) calculated for 10 initial conditions in the representative plane. Their locations, superimposed to the MEGNO-map, are shown in the upper frame, while the time evolution of their LCE is shown in the bottom plot. Along with the evolution of their LCE, we have plotted

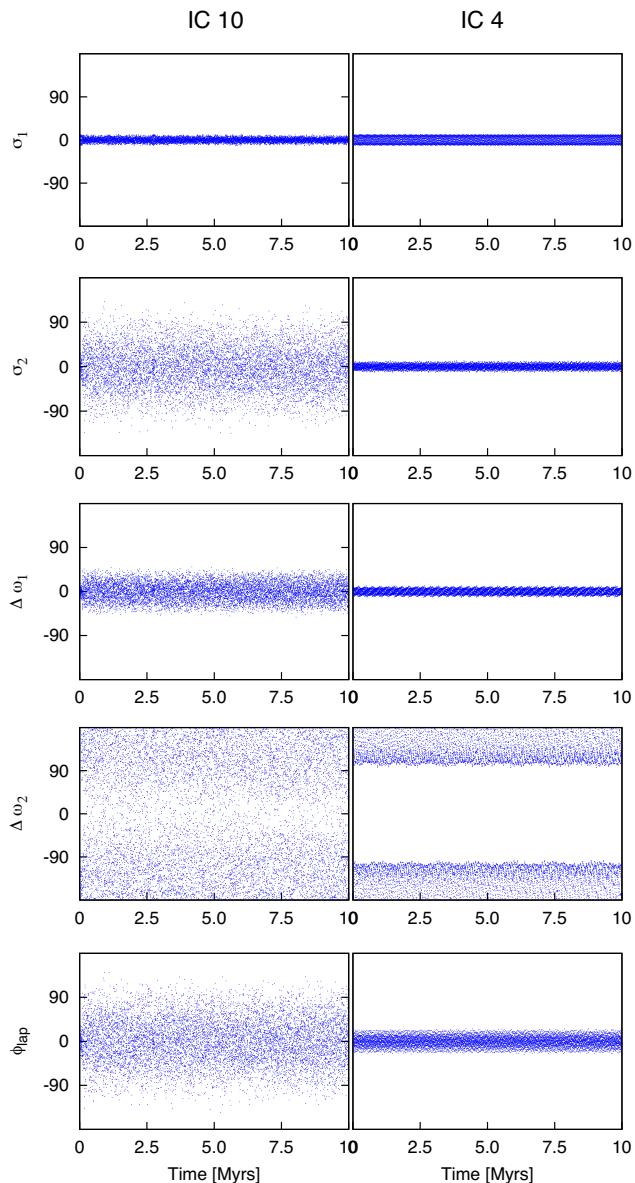


**Figure 7.** Time evolution of the resonant angles corresponding to initial conditions IC 10 and IC 4 described in Fig. 6. These show the evolution of two characteristic conditions placed at the inner (IC 4) and at the outer (IC 10) resonant regions.

the corresponding evolution of the initial conditions represented by the co-planar orbital fits already mentioned in Section 4.1.

All the initial conditions set in the outer resonant region (IC 7 through IC 10) are characterized by very large values of LCE, of the order of  $10^{-1} \text{ yr}^{-1}$ , corresponding to extremely chaotic motion. However, as shown in the left-hand panels of Fig. 7 for IC 10, there is no indication of orbital instability, at least within several  $10^7$  yr. The system is inside the Laplace resonance, although the resonant angle displays large-amplitude librations. The resonant angles of the individual two-body resonances are also librating, and the behaviour of  $\Delta\varpi_1$  indicates that  $m_1$  and  $m_2$  are trapped in an Apsidal Corotation Resonance (ACR; Beaugé, Ferraz-Mello & Micht 2003). The difference in longitudes of pericentre of the outer

pair ( $\Delta\varpi_2$ ), however, circulates, indicating that this sub-system is not in an ACR.

These values of LCE are very similar to those obtained by Batygin et al. (2015), where they estimate a Lyapunov time for Rivera’s orbital fit using the aforementioned 2D model. In fact, all orbital fits show a similar behaviour (see Fig. 6), with values of LCE somewhere between those corresponding to the IC7–IC10 and IC2–IC5–IC6 groups of initial configurations.

Continuing with Fig. 6, initial conditions placed in the red streaks within the inner resonant region (IC 2, 5, and 6) have moderate values of LCEs. While these are significantly smaller than before, they still correspond to significant chaotic motion. Finally, the initial conditions placed inside the relatively regular inner resonant region (IC 1, 3, and 4) all show almost identical very small values of the Lyapunov exponent. At the end of the simulation, at  $T = 1.2 \times 10^7$  yr, the value of LCE has yet to reach a plateau, indicating that this region is characterized by very regular motion. Indeed, the theoretical expected final value of the LCE for regular motion is  $\ln T/T \sim 10^{-6}$ .

The right-hand frames of Fig. 7 shows the time evolution of the resonant angles for IC 4. All, together with differences in longitudes of pericentre, exhibit small-amplitude librations, indicating that this configuration is not only trapped inside the Laplace resonance but also exhibits a double ACR. The same is noted for the other initial conditions in this region. This seems to indicate that the difference in dynamics between the inner and outer resonant domains is defined by the behaviour of the auxiliary resonant angles, particularly that of the outer pair. Thus, it appears that the almost regular region deep within the Laplace resonance corresponds to Double-ACR orbits, while the highly chaotic outer region is associated to an ACR for the inner pair and a  $\sigma_2$ -libration of the outer pair of planets.

## 7 CONCLUSIONS

The choice of the GJ-876 system, although arbitrary, is due to two main factors. On one hand, we want to analyse the diffusive process and chaotic mixing in a system which could have avoided other chaotic processes during its early stages after gas depletion. In this sense, GJ-876 is a well-characterized system that displays a resonant chain of planetary bodies. On the other hand, a natural motivation was the extensive quantity of previous works where this specific planetary system has been used as prime example.

We have started our analysis by improving our representation of the region covered by the Laplace resonance in the  $(a_3, e_3)$  plane. We integrated one order of magnitude more initial conditions than we had previously done, and also extended the total integration time for each to  $2 \times 10^5$  yr. We therefore explored in a very precise way the main dynamical structures that this system represents.

As was already pointed out in Marti et al. (2013), we recognized two main regions in the surroundings of the resonance. The one we called inner resonant region is characterized by lower values of  $\Delta e_3$ , a MEGNO indicator value of  $\langle Y \rangle \sim 2$  and utterly very small values for the LCE which result in seemingly large Lyapunov times. The outer resonant region is, however, dominated by extremely chaotic dynamics, presenting high values of  $\Delta e_3$  and  $\langle Y \rangle$ , and having LCE’s somewhat higher than in the inner region. Moreover, we also concluded that the inner zone corresponds very well with the region of lower libration amplitude of the resonant angle  $\phi_{\text{lap}}$ . This feature, although trivial, is extremely important because it shows that the multiresonant configuration of the four-body system ( $m_0 + m_i$ ,  $i = 1, 3$ ) is responsible for its long-term stability. The coincidence in the low-amplitude libration regions of  $\sigma_2$  and  $\phi_{\text{lap}}$  on the phase

space allows us to state that the system is unable to show a libration of the Laplace angle without being trapped in the two single two-body resonances.

Although both the MEGNO and  $\Delta e_3$  indicators point towards chaoticity within the inner resonant region, this characteristic should be considered with care. Indeed, we have already stated that aside the overall chaoticity of the system, we could still define regions with completely different dynamical behaviours. The higher precision used in our grid-simulations of initial conditions allowed us to perform a much more detailed map of the inherent chaotic structure inside the Laplace resonance. As it was shown in the bottom frame of Fig. 2, several thin strips of higher values of  $\langle Y \rangle$  cross each other along the whole inner domain. This behaviour is completely expected (see Section 4.2) due to the overlapping of resonances associated with slight variations of the longitudes of perihelion of the planets, which are located at the same region as the Laplace resonance.

In order to get a quantitative idea of how the different aspects of chaotic behaviour affect the dynamics of the system and its resonant structure, we performed numerical calculations concerning the diffusive process, which occur inside the multiresonance domain. Although diffusion is always present, we show here that the rate at which the local variation of fundamental parameters ( $a_3$ ,  $e_3$ ) associated with the actions in phase space (see Section 3), is completely limited to the inner region of the resonance as long as their initial values reside in that domain. In a few cases where the initial conditions were located at the borders of the inner region or at the strips of moderate chaos, the diffusion rate seems to be higher. We also performed calculations of the diffusive process for an ensemble of initial conditions located outside the inner resonant region, yielding a time evolution of the variance very close to normal diffusion [i.e.  $\alpha = 0.942715$  in the model  $\sigma^2(t) = ct^\alpha$ ], while for any of the other ensembles the fit of this exponent was seemingly smaller. This result clearly shows that the assumption of normal diffusion ( $\sigma_2(t) \propto t$ ) for these kinds of systems is not well sustained.

The LCE calculated for 10 different initial conditions, chosen to represent some crucial aspects of the resonance, are clearly in accordance with the overall analysis developed here. There is a direct link between the lower values of LCE and initial conditions at the inner zone. Accordingly, for systems with initial conditions placed outside the inner part, they not only reached higher values of LCE, but they also reach these values at earlier times than systems with initial conditions at the inner region. Moreover, those conditions which were located specifically at the moderate MEGNO strips, show an intermediate value of LCE, and even some, seem not to have reached its asymptotic LCE value at the final time of the simulation.

The LCE obtained by Batygin et al. (2015) corresponds to the outer resonant region of the Laplace resonance, as they make use of the fit from Rivera et al. (2010, see also Table 1). However, we found that the inner region, characterized by a Double-ACR and small amplitude of librations of the resonant angles, contains initial conditions which are less chaotic, associated with Lyapunov times larger than  $10^5$  yr. In fact we have run a simulation of Rivera's orbital fit, which led to a Lyapunov time of  $\sim 100$  yr. Our integrations for initial conditions in the inner resonant region which are not specifically on any of the moderate MEGNO strips, are not only stable for more than  $10^7$  yr, they also show a much more limited evolution of the libration amplitudes of the resonant angles (see right-hand frame of Fig. 7), as well as a much regular variation. This strongly suggests that although chaotic, the system could and in fact has long-term stability, and that chaotic mixing should not

have occurred in systems which display resonant dynamics similar to that of GJ-876.

Although this research was developed for a specific planetary system, it seems reasonable that the main characteristics of any system representing similar multiresonant configurations could share the main features that were described throughout this paper. The implementations, although numerically expensive, should not carry major problems, and so, an extension to any such a system would only need a sufficiently precise orbital fit. As the number of multiresonant systems is constantly increasing, this type of dynamical study is of fundamental importance mainly for stability considerations, and secondly because of the constraints that multiresonant planetary systems can impose on the planetary formation theories.

## ACKNOWLEDGEMENTS

This work used computational resources from CCAD – Universidad Nacional de Córdoba (<http://ccad.unc.edu.ar/>), in particular the Mendieta Cluster, which is part of SNCAD MinCyT, República Argentina. Other numerical simulations were made on the local computing resources from the Instituto de Astronomía Teórica y Experimental (IATE), at the University of Córdoba (Córdoba, Argentina) and also on the IFLySIB computational resources at the Instituto de Física de Líquidos y Sistemas Biológicos–CONICET–UNLP. We also want to thank the Instituto de Astrofísica de La Plata (IALP)–CONICET–UNLP, La Plata, for supporting this research.

The authors also wish to express their gratitude to an anonymous referee for important suggestions and comments.

## REFERENCES

- Arnol'd V. I., 1963, *Russ. Math. Surv.*, 18, 9  
 Arnol'd V. I., 1964, *Sov. Math. Dokl.*, 5, 581  
 Baluev R. V., 2011, *Celest. Mech. Dyn. Astron.*, 111, 235  
 Batygin K., Deck K. M., Holman M. J., 2015, *AJ*, 149, 167  
 Beaugé C., Nesvorný D., 2012, *ApJ*, 751, 119  
 Beaugé C., Ferraz-Mello S., Micht T., 2003, *ApJ*, 593, 1124  
 Cachucho F., Cincotta P. M., Ferraz-Mello S., 2010, *Celest. Mech. Dyn. Astron.*, 108, 35  
 Chambers J. E., Wetherill G. W., Boss A. P., 1996, *Icarus*, 119, 261  
 Chirikov B. V., 1979, *Phys. Rep.*, 52, 263  
 Chirikov B. V., Vecheslavov V. V., 1993, *J. Stat. Phys.*, 71, 243  
 Cincotta P. M., 2002, *New Astron. Rev.*, 46, 13  
 Cincotta P. M., Simó C., 2000, *A&AS*, 147, 205  
 Cincotta P. M., Giordano C. M., Simó C., 2003, *Physica D: Nonlinear Phenom.*, 182, 151  
 Cincotta P. M., Efthymiopoulos C., Giordano C. M., Mestre M. F., 2014, *Physica D: Nonlinear Phenom.*, 266, 49  
 Deck K. M., Payne M., Holman M. J., 2013, *ApJ*, 774, 129  
 Fabrycky D. C. et al., 2012, *ApJ*, 750, 114  
 Ford E. B., Kozinsky B., Rasio F. A., 2000, *ApJ*, 535, 385  
 Giordano C. M., Cincotta P. M., 2004, *A&A*, 423, 745  
 Giorgilli A., 1990, in Benest D., Froeschle C., eds, *Modern Methods in Celestial Mechanics. Comptes Rendus de la 13ieme Ecole Printemps d'Astrophysique de Goutelas, France.* p. 249  
 Giuppone C. A., Morais M. H. M., Correia A. C. M., 2013, *MNRAS*, 436, 3547  
 Froeschlé C., Guzzo M., Lega E., 2006, *Nonlinearity*, 19, 1049  
 Hands T. O., Alexander R. D., Dehnen W., 2014, *MNRAS*, 445, 749  
 Jurić M., Tremaine S., 2008, *ApJ*, 686, 603  
 Laskar J., 1989, *Nature*, 338, 237  
 Laskar J., Robutel P., 1995, *Celest. Mech. Dyn. Astron.*, 62, 193  
 Laughlin G., Adams F. C., 1998, *ApJ*, 508, L171  
 Lega E., Guzzo M., Froeschle C., 2003, *Physica D: Nonlinear Phenom.*, 182, 179

- Lochak P., 1999, Hamiltonian systems with Three of More Degrees of Freedom. Kluwer, Dordrecht
- Marchal C., Bozis G., 1982, *Celest. Mech.*, 26, 311
- Marchal C., Saari D. G., 1975, *Celest. Mech.*, 12, 115
- Martí J. G., Beaugé C., 2015, *Int. J. Astrobiology*, 14, 313
- Martí J. G., Giuppone C. A., Beaugé C., 2013, *MNRAS*, 433, 928
- Masset F., Snellgrove M., 2001, *MNRAS*, 320, L55
- Morbidelli A., Tsiganis K., Crida A., Levison H. F., Gomes R., 2007, *AJ*, 134, 1790
- Nekhoroshev N. N., 1977, *Russ. Math. Surv.*, 32, 1
- Nesvorný D., Morbidelli A., 1999, *Celest. Mech. Dyn. Astron.*, 71, 243
- Ramos X. S., Correa-Otto J. A., Beaugé C., 2015, *Celest. Mech. Dyn. Astron.*, 123, 453
- Rasio F. A., Ford E. B., 1996, *Science*, 274, 954
- Rivera E. J., Laughlin G., Butler R. P., Vogt S. S., Haghighipour N., Meschiari S., 2010, *ApJ*, 719, 890
- Rowe J. F. et al., 2014, *ApJ*, 784, 45
- Smith A. W., Lissauer J. J., 2009, *Icarus*, 201, 381
- Wang S., Ji J., Zhou J.-L., 2012, *ApJ*, 753, 170
- Weidenschilling S. J., Marzari F., 1996, *Nature*, 384, 619
- Wisdom J., 1980, *AJ*, 85, 1122

This paper has been typeset from a  $\text{\TeX}/\text{\LaTeX}$  file prepared by the author.